Superradiant Topological Peierls Insulator inside an Optical Cavity

Farokh Mivehvar, Helmut Ritsch, and Francesco Piazza*
Institut für Theoretische Physik, Universität Innsbruck, A-6020 Innsbruck, Austria
(Received 17 November 2016; published 16 February 2017)

We consider a spinless ultracold Fermi gas tightly trapped along the axis of an optical resonator and transversely illuminated by a laser closely tuned to a resonator mode. At a certain threshold pump intensity, the homogeneous gas density breaks a $\mathbf{Z}_2$ symmetry towards a spatially periodic order, which collectively scatters pump photons into the cavity. We show that this known self-ordering transition also occurs for low field seeking fermionic particles when the laser light is blue detuned to an atomic transition. The emergent superradiant optical lattice in this case is homopolar and possesses two distinct dimerizations. Depending on the spontaneously chosen dimerization, the resulting Bloch bands can have a nontrivial topological structure characterized by a nonvanishing Zak phase. In the case where the Fermi momentum is close to half of the cavity-mode wave number, a Peierls-like instability here creates a topological insulator with a gap at the Fermi surface, which hosts a pair of edge states. The topological features of the system can be nondestructively observed via the cavity output: the Zak phase of the bulk coincides with the relative phase between laser and cavity field, while the fingerprint of edge states can be observed as additional broadening in a well-defined frequency window of the cavity spectrum.

DOI: 10.1103/PhysRevLett.118.073602

Introduction.—The experimental progress in coupling ultracold quantum gases to the electromagnetic field of high-Q cavities [1–8] has opened a new avenue for creating and exploring novel many-body collective phenomena in the framework of cavity QED [9–16]. One hallmark effect of the coupled atom-field dynamics is self-ordering, where the atoms spontaneously break the translational symmetry and form a spatial pattern, which maximizes collective (i.e., superradiant) scattering of the pump photons into the cavity [1,5–7,17,18]. The interplay between light-induced long-range interactions, the quantum statistics of the particles [19–26], and short-range interatomic interactions [27–33] gives rise to a wealth of intriguing phenomena. Corresponding experiments have become successful quantum simulators for Bose-Hubbard models with infinitely long-range interactions demonstrating the Dicke superradiant phase transition as well as a supersolid phase [34–36].

Recent theoretical developments have highlighted a further possibility to exploit cavity fields to generate artificial spin-orbit coupling [37–41] or dynamical gauge fields [42–46], exploiting Raman processes involving a cavity mode to induce internal transitions between two atomic ground-state sublevels (pseudospins) [38,41] or tunneling between two sites of a preexisting lattice [42,43,45]. As a consequence, self-organized phases are predicted to become topological when the artificial spin-orbit coupling or the gauge field is mediated by the superradiant cavity light [41–43].

In this Letter, we present a configuration leading to topologically nontrivial self-ordered phases for spin-polarized fermionic atoms in one dimension without artificial spin-orbit coupling or gauge fields. We consider the same experimental setup exploited to observe the superradiant self-ordering transition of bosons [1,5–7], involving transversely laser-driven atoms coupled to a single mode of an optical resonator in the dispersive regime (see Fig. 1). The motion of the atoms transverse to the cavity axis is frozen by a cigar-shaped dipole trap [35]. The superradiant lattice formed from the interference between the laser and the

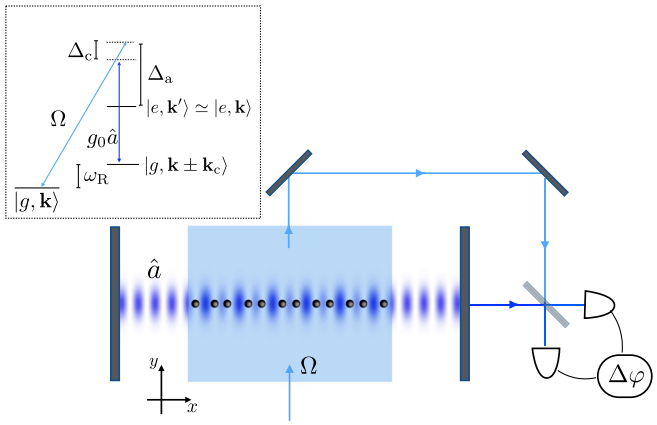

FIG. 1. Schematic view of fermionic atoms trapped in a one-dimensional elongated tube along the axis of an optical resonator and driven by a transverse blue-detuned ($\Delta_a > 0$ with respect to an atomic transition $g \leftrightarrow e$) laser with Rabi frequency Ω. Δ_c denotes detuning with respect to a standing-wave cavity mode. The atoms are low field seekers trapped at the light intensity minima generated by the interference of the cavity field and the plane-wave transverse pump laser. The relative phase $\Delta\varphi$ of the cavity output and the pump laser corresponds to the Zak phase of the lattice bands in real time (see Fig. 2). (Inset) The coupling of momentum states via pump and cavity fields.

cavity field is dimerized; i.e., the unit cell contains two lattice sites. During self-ordering, the particles choose between the two possible dimerizations in a spontaneous $\mathbf{Z}_2$-symmetry breaking process. The nature of the dimerized superradiant lattice qualitatively depends on the sign of the laser-atom detuning Δ_a. For the conventional red detuning $\Delta_a < 0$, dimerization is heteropolar (i.e., there is a finite energy offset between the two sites in the unit cell), while, for blue detuning $\Delta_a > 0$, on which we focus in the following, it is homopolar (zero offset) [47]. The dimerized-lattice bands can have a nontrivial topological structure characterized by their Zak phase φ_{Zak}, which is the Berry's phase picked up by moving adiabatically through the entire first Brillouin zone [48]. In the homopolar (blue-detuned) case, φ_{Zak} is $\mathbf{Z}_2$ quantized and can be either 0 or π, depending on the (in our case spontaneously chosen) dimerization.

Our model shares several features with the Su-Schrieffer-Heeger (SSH) [49] and Holstein [50] models, describing electrons coupled to lattice phonons. The role of the phononic degrees of freedom is played in our scheme by a single global cavity mode. Specifically, if the Fermi momentum is close to half of the cavity-mode wave vector, an energy gap opens at the Fermi surface of the dimerized superradiant lattice [24]. For one of the two possible dimerizations, the system enters a topological phase with chiral symmetry, hosting a pair of edge states within the energy gap in the finite system [51,52]. This mechanism is analogous to the Peierls instability, whereby a one-dimensional solid-state crystal spontaneously dimerizes into an insulator due to the electron-phonon coupling [53]. This aspect is absent in the free-space realization of the superlattice in Ref. [54], where the dimerized lattice is merely a static optical potential without phononic degrees of freedom.

We also demonstrate how the signatures of the nontrivial topology in our open system can be nondestructively read out in real time simply by monitoring the cavity output. The Zak phase directly appears as the relative phase $\Delta\varphi$ between the laser and the cavity field, which is an easily accessible quantity [55]. In addition, in a finite system, the edge states can be detected in the cavity spectrum since their presence introduces additional broadening in a specific well-defined frequency window.

Model and approach.—Consider laser-driven ultracold spin-polarized fermions in a standing-wave resonator similar to the one shown in Fig. 1. The system is effectively described by the Hamiltonian [10]

$$\hat{H} = \int dx \hat{\psi}^\dagger \Big(-\frac{\hbar^2}{2m}\frac{d^2}{dx^2} + \hbar\eta\cos(k_c x)(\hat{a}e^{-i\varphi_\Omega} + \mathrm{H.c.}) + U_0\cos^2(k_c x)\hat{a}^\dagger\hat{a} \Big)\hat{\psi} - \hbar\Delta_c\hat{a}^\dagger\hat{a}, \quad (1)$$

where the atomic excited state has been adiabatically eliminated (dispersive regime of a large Δ_a) and the atomic motion is restricted to one dimension along the cavity axis x. We assume plane-wave laser illumination and a standing-wave cavity mode proportional to $\cos(k_c x)$ with a wave number k_c. In Eq. (1) we introduced the optical potential depth per photon $U_0 \equiv \hbar g_0^2/\Delta_a$ equivalent to the cavity frequency shift per atom, the effective pump strength $\eta \equiv g_0|\Omega|/\Delta_a$, the laser phase φ_Ω and the cavity detuning with respect to the pump frequency Δ_c. Here, g_0 and Ω are the atom-cavity coupling and the single-photon Rabi frequency, respectively, and H.c. stands for the Hermitian conjugate. The recoil energy $E_R \equiv \hbar^2 k_c^2/2m$ and cavity wave number k_c are the natural units of energy and momentum here. Finally, $\hat{a}$ is the cavity photon bosonic annihilation operator and $\hat{\psi}(x)$ is the atomic fermionic field operator.

The $\mathbf{Z}_2$-symmetry transformation $x \to x \pm \pi/k_c$, $\hat{a} \to -\hat{a}$, $\hat{a}^\dagger \to -\hat{a}^\dagger$ leaves the Hamiltonian (1) invariant. This symmetry is spontaneously broken at the self-ordering transition where the cavity mode develops a finite coherent amplitude $\alpha = \langle\hat{a}\rangle = |\alpha|\exp(i\varphi_\alpha)$, and its phase is locked to the laser phase φ_Ω by a Josephson-like energy term $E_J(\alpha) \propto -N\eta^2\rho|\alpha|^2\cos^2(\Delta\varphi)$, with $\rho = N/L$ being the average atomic density [20]. E_J fixes the relative phase $\Delta\varphi = \varphi_\alpha - \varphi_\Omega$ to being either 0 or π (see Fig. 2). In the thermodynamic limit, $N, L \to \infty$, $\rho = \mathrm{const}$, the superradiant phase is exactly described by a mean-field approach where only the coherent field component α is retained and satisfies the following self-consistent equations [20]:

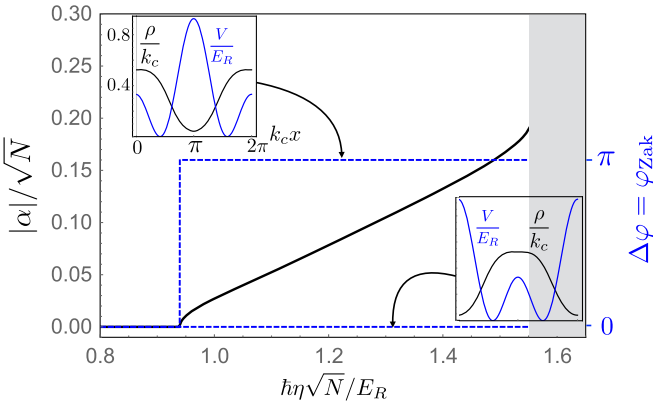

FIG. 2. Spontaneous $\mathbf{Z}_2$-symmetry breaking at the superradiant self-ordering transition in the configuration of Fig. 1 seen via the modulus of coherent cavity-field amplitude (the solid line) as a function of the pump strength η. The blue dashed line shows the cavity phase $\Delta\varphi$ relative to the driving laser, for which we have either $\Delta\varphi = 0$ or $\Delta\varphi = \pi$ depending on the lattice dimerization. (Insets) Corresponding atomic densities (the black solid line) and lattice potential (rescaled by 0.5, the blue solid line) within a unit cell, for $\hbar\eta\sqrt{N} = 1.55E_R$. $\Delta\varphi$ coincides with the Zak phase φ_{Zak} of the lowest Bloch band. The gray-shaded area denotes an unstable region of the system (see Fig. 3). Results are obtained for spin-polarized fermions with the parameters $k_F = k_c/2$, $k_B T = 0.01E_R$, $\hbar\Delta_c = 12E_R$, $U_0 N = 32.35E_R$.

$$\alpha = \frac{1}{\Delta_c}\int dx\rho(x)\frac{\partial V_{\rm sl}(x)}{\partial \alpha^*}, \qquad \int dx\rho(x) = N, \quad (2)$$

with the superradiant lattice potential

$$V_{\rm sl}(x) = U_0|\alpha|^2\cos^2(k_c x) + 2\hbar\eta|\alpha|\cos(\Delta\varphi)\cos(k_c x), \quad (3)$$

and the atomic density

$$\rho(x) = \langle\hat{\psi}^\dagger(x)\hat{\psi}(x)\rangle = \sum_n \int_{\rm BZ}\frac{dk}{2\pi} n_F[\epsilon_n(k)]|\psi_{n,k}(x)|^2. \quad (4)$$

Here, $n_F(\epsilon) = \{1+\exp[\beta(\epsilon-\mu)]\}^{-1}$ is the Fermi-Dirac distribution, and $\epsilon_n(k)$ and $\psi_{n,k}(x)$ are, respectively, the Bloch eigenenergies and the eigenstates of the single-particle Hamiltonian with the superradiant lattice potential $V_{\rm sl}(x)$, whose periodicity $2\pi/k_c$ defines the Brillouin zone BZ $= [-k_c/2, k_c/2]$. The chemical potential is fixed by the second equation in Eq. (2). We stress that the dependence of $\rho(x)$ on α through the dynamical lattice $V_{\rm sl}(x)$ requires a self-consistent solution for α and μ in Eq. (2).

Dealing with an open system, one should, in principle, include photon losses at the rate κ out of the cavity [9]. However, the induced heating rates of the Fermi gas are ineffective up to long time scales proportional to the atom number N, as shown in Ref. [25]. Within the superradiant phase, the photon losses introduce damping of the coherent-field amplitude, which follows the momentary atomic distribution with a phase shift that can be made vanishingly small for $\Delta_c \gg \kappa$ [55]. Even though the superradiant self-ordering transition becomes dissipative [56,57], the $\mathbf{Z}_2$ nature of the symmetry breaking is not affected.

Emergent dimerized superradiant lattice.—The solution of Eq. (2) is shown in Fig. 2. Above a critical pump strength (see also Fig. 3), the coherent part of the cavity field α grows monotonically, with its relative phase $\Delta\varphi$ locked at either 0 or π, breaking the $\mathbf{Z}_2$ symmetry. The two cases correspond to two possible lattice dimerizations, as shown by Eq. (3) and in the inset of Fig. 2 within one unit cell.

The one-dimensional bands can be characterized by the Zak phase [48,58],

$$\varphi_{\rm Zak}^{(n)} = k_c\int_{\rm BZ} dk\int_0^{2\pi/k_c} dx u_{n,k}^*(x)\frac{\partial u_{n,k}(x)}{\partial k} \overset{n=1}{=} \Delta\varphi, \quad (5)$$

where $u_{n,k}(x) = \exp(-ikx)\psi_{n,k}(x)$ is the periodic part of the Bloch wave function. The Zak phase is, in general, not quantized, and it can take any value between zero and 2π. That said, in the presence of chiral symmetry (as for the blue-detuned, homopolar lattice considered here), it is $\mathbf{Z}_2$ quantized and can assume solely the values 0 or π. The Zak phase $\varphi_{\rm Zak}$ of the lowest Bloch band $n = 1$ coincides with the relative phase of the cavity $\Delta\varphi$, as indicated in the last equality of Eq. (5), in the case of a mirror symmetric choice for the unit cell (see the inset of Fig. 2). The mirror symmetric choice of the unit cell, though not a unique choice [54,59], corresponds to the Wigner-Seitz cell, and the Zak phase can then be interpreted as a topological invariant. The nonvanishing Zak phase $\varphi_{\rm Zak} = \pi$ indeed signals a nontrivial topological band, which hosts localized zero-dimensional edge states in a finite system. This is illustrated in the inset of Fig. 4, showing the low-lying energy spectrum of a finite lattice consisting of 50 unit cells of the topologically nontrivial dimerization. A smooth polynomial wall potential $V_{\rm wall}(x) = V_0(x^2+x^4+x^6)$ is added to both ends of the finite lattice, with $V_0/E_R = 150$. The two isolated eigenenergies in the midgap correspond to the two localized edge states. They are quite robust with respect to variation of the wall potential in the range $V_0/E_R \sim 1-10^4$. However, they lie around midgap only for $V_0/E_R \sim 10^2$.

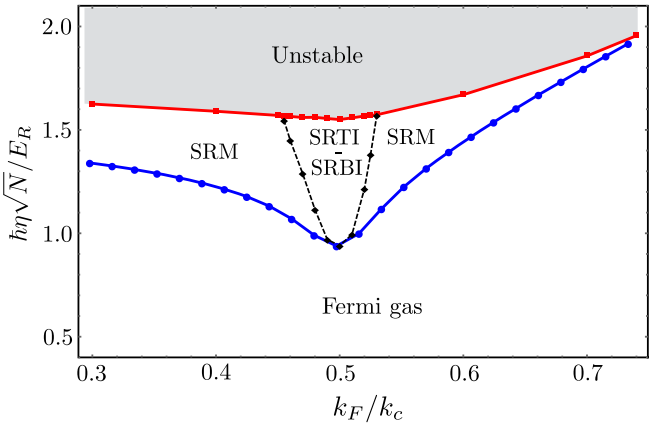

FIG. 3. Phase diagram in the $\eta - k_F$ plane. For a strong enough pump η (above the blue line), the system self-orders into a superradiant pattern. In the self-ordered phase, the system is in either a SRM phase or an insulator state. The superradiant insulating phase, in turn, is either a SRBI or a SRTI, characterized by their Zak phases (see Fig. 2). At the half filling $k_F = k_c/2$, we have a direct phase transition between the uniform Fermi gas and the SRBI or SRTI. Otherwise, this phase transition occurs only through the SRM phase. For an even stronger drive (above the red line) the self-ordered phase becomes unstable. The parameters are the same as in Fig. 2.

Measuring topological invariants directly is often challenging and requires nonlocal probes, as, for instance, the Bloch-Ramsey interferometric technique employed to measure the Zak phase with ultracold atoms in a superlattice [54]. In our setup, where the lattice (3) is formed through the interference between the laser and the superradiant cavity field, $\varphi_{\rm Zak}$ can be continuously and nondestructively read out as the relative phase $\Delta\varphi$ between the pump and cavity fields, as is schematically depicted in Fig. 1.

Topological insulator.—Figure 3 shows the phase diagram in the parameter space of the effective pump strength

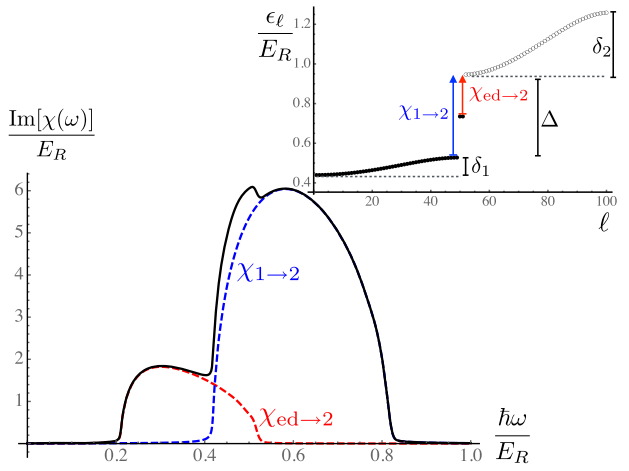

FIG. 4. Signature of the edge states in the absorption spectrum of the SRTI phase with respect to the propagation of cavity photons. The imaginary part of the polarization [Eq. (6)] as a function of frequency is shown for a finite system encompassing 50 unit cells at half filling. The total absorption χ (the black solid line) has two contributions: $\chi_{\mathrm{ed}\to2}$ (the red dashed line) is due to the presence of edge states, while $\chi_{1\to2}$ (the blue dashed line) is present also without edge states. (Inset) The atomic energy spectrum, where filled (empty) circles indicate occupied (empty) states. The two isolated eigenenergies in the midgap correspond to the two localized edge states. The parameters are the same as in Fig. 2, with $\hbar\eta\sqrt{N} = 1.55E_R$.

$\hbar\eta\sqrt{N}/E_R$ versus the Fermi momentum k_F/k_c. For densities around the half filling $k_F = k_c/2$, with $k_F = \pi\rho$, the superradiant phase corresponds to an insulator, while sufficiently away from this point the system is found in a superradiant metallic (SRM) phase. The dashed lines in Fig. 3 indicate the continuous crossover from the metallic to the insulating phase. The transition to an insulator within a dimerized lattice at half filling follows the same mechanism underlying the Peierls instability in one-dimensional electron-phonon models [49,53]. The critical pump strength for the superradiant transition vanishes at $T = 0$, as noted previously for red-detuned superradiant lattices [22–24]. The superradiant insulating phase has a band gap Δ that is proportional to the absolute value of the cavity-field amplitude $|\alpha|$. The superradiant insulator phase can be either a (topologically trivial) band insulator (SRBI) for $\Delta\varphi = 0$ or a topological insulator (SRTI) for $\Delta\varphi = \pi$. For the latter case, the lattice bands host a pair of edge states in the finite system, as discussed above. The SRTI possesses chiral (or sublattice) symmetry [60] and belongs to the AIII class introduced in Ref. [52]. In the tight-binding limit, particle-hole and time-reversal symmetries are additionally present, putting the SRTI in the BDI class of Ref. [52], i.e., in the same class as the SSH model.

Increasing the pump amplitude η further, the system reaches a second transition point where no stable solutions of Eq. (2) can be found anymore, as indicated by the gray-shaded areas in Figs. 2 and 3. This instability is caused by the competition between the $\propto\cos(k_c x)$ and the $\propto\cos^2(k_c x)$ contribution to the superradiant lattice potential in Eq. (3) and is characteristic of the blue-detuned homopolar lattice. As shown in Ref. [47], this instability can correspond to the onset of the limit cycle and even chaotic behavior.

Detecting edge states.—As described above, in a finite system, the SRTI phase possesses a pair of topological edge states within the band gap, which can be directly observed in the spectral properties of the cavity output. This can be verified by computing the optical polarizability $\chi(\omega)$ of the SRTI in the finite system. $\chi(\omega)$ corresponds to the dynamic response function of the medium with respect to density perturbations induced by cavity photons and reads [61]

$$\chi(\omega) = \sum_{\ell,\ell'} \frac{n_F(\epsilon_\ell) - n_F(\epsilon_{\ell'})}{\hbar\omega + \epsilon_\ell - \epsilon_{\ell'} + i0^+} \left| \int dx \psi_\ell^* \frac{\partial V_{\mathrm{sl}}(x)}{\partial \alpha^*} \psi_{\ell'} \right|^2, \tag{6}$$

where ϵ_ℓ and $\psi_\ell(x)$ are the eigenenergies and eigenstates of the single-particle Hamiltonian with the potential $V_{\mathrm{sl}}(x) + V_{\mathrm{wall}}(x)$. The real (imaginary) part of χ corresponds to the atomic dispersion (absorption) with respect to the propagation of cavity photons.

Using the identity $\mathrm{Im}[1/(\hbar\omega + \epsilon_\ell - \epsilon_{\ell'} + i0^+)] = -\pi\delta(\hbar\omega + \epsilon_\ell - \epsilon_{\ell'})$, one can see that the medium absorbs photons only if energy is conserved in the transition between two eigenstates (one of which must be occupied) having a finite matrix element with respect to the operator $\partial V_{\mathrm{sl}}/\partial\alpha^*$. In the absence of edge states, the Fermi medium absorbs cavity photons only for frequencies $\hbar\omega \geq \Delta$, where Δ is the energy gap between low-lying filled valence states and upper empty conduction states (see the inset in Fig. 4) and is assumed to be much larger than the temperature, $k_B T \ll \Delta$. On the other hand, when edge states are present in the middle of the gap, the medium can absorb photons with even lower energy: $\hbar\omega \geq \Delta/2$. This holds as long as the matrix element is nonvanishing. By increasing the length of the system L, the edge-state contribution $\chi_{\mathrm{ed}\to2}(\omega)$ to the total response function $\chi(\omega)$ decreases like $1/L$ in the thermodynamic limit $N/L = \mathrm{const}$, where also $U_0 \propto 1/L$ and $\eta \propto 1/\sqrt{L}$. The edge states indeed contribute to absorption only locally.

Figure 4 shows the imaginary part of $\chi(\omega)$. The blue (red) dashed curve indicates $\chi_{1\to2}$ ($\chi_{\mathrm{ed}\to2}$), the contribution of transitions from filled lowest valence (edge) states into upper empty conduction states. It is evident that the presence of edge states in the SRTI phase drastically modifies the polarization function and opens an additional absorption channel in the well-defined frequency range $\Delta/2 \leq \hbar\omega \leq \Delta/2 + \delta_2$, with δ_2 being the conduction bandwidth. We note that, for $\delta_2 < \Delta/2$, this additional absorption window becomes even fully separated from the one related to transitions between valence and conduction

states. This provides experimental means to detect edge states via a nondestructive measurement since the absorption $\mathrm{Im}[\chi(\omega)]$ influences the broadening of the cavity resonance and can, for instance, be extracted from the width of the peak of the incoherent fluorescence spectrum or probe-transmission spectrum [25]. The bad-cavity regime (i.e., the large photon-loss rates κ) can be optimal since all of the spectral weight is then concentrated around an almost purely atomic resonance located at low frequencies, whose width is approximately given by the atomic absorption $\mathrm{Im}[\chi]$ plus a small correction inversely proportional to κ [25].

Conclusions.—We introduced and characterized a simple configuration of fermionic atoms trapped along the axis of an optical cavity to implement a genuine topological self-organized superradiant state. The proposed setup is already experimentally available. Remarkably, the configuration features built-in nondestructive monitoring tool via the cavity output photons, which allows us to directly probe topological properties of the system like the Zak phase and the existence of the edge states. This could, for instance, allow us to directly verify the topological bulk-boundary correspondence. This would require us to measure both the Zak phase and the spectral signature of edge states within a *single* experimental realization, which is impossible with destructive measurements.

We thank Johannes Lang for the fruitful discussions. F. P. acknowledges the support of the APART fellowship of the Austrian Academy of Sciences. F. M. and H. R. are supported by Austrian Science Fund Project No. I1697-N27.

*Corresponding author.
francesco.piazza@uibk.ac.at

[1] A. T. Black, H. W. Chan, and V. Vuletić, Phys. Rev. Lett. **91**, 203001 (2003).
[2] S. Slama, S. Bux, G. Krenz, C. Zimmermann, and P. W. Courteille, Phys. Rev. Lett. **98**, 053603 (2007).
[3] Y. Colombe, T. Steinmetz, G. Dubois, F. Linke, D. Hunger, and J. Reichel, Nature (London) **450**, 272 (2007).
[4] S. Gupta, K. L. Moore, K. W. Murch, and D. M. Stamper-Kurn, Phys. Rev. Lett. **99**, 213601 (2007).
[5] K. Baumann, C. Guerlin, F. Brennecke, and T. Esslinger, Nature (London) **464**, 1301 (2010).
[6] K. J. Arnold, M. P. Baden, and M. D. Barrett, Phys. Rev. Lett. **109**, 153002 (2012).
[7] H. Keßler, J. Klinder, M. Wolke, and A. Hemmerich, Phys. Rev. Lett. **113**, 070404 (2014).
[8] A. J. Kollar, A. T. Papageorge, K. Baumann, M. A. Armen, and B. L. Lev, New J. Phys. **17**, 043012 (2015).
[9] H. Ritsch, P. Domokos, F. Brennecke, and T. Esslinger, Rev. Mod. Phys. **85**, 553 (2013).
[10] C. Maschler, I. B. Mekhov, and H. Ritsch, Eur. Phys. J. D **46**, 545 (2008).
[11] S. Gopalakrishnan, B. L. Lev, and P. M. Goldbart, Nat. Phys. **5**, 845 (2009).
[12] S. Gopalakrishnan, B. L. Lev, and P. M. Goldbart, Phys. Rev. Lett. **107**, 277201 (2011).
[13] P. Strack and S. Sachdev, Phys. Rev. Lett. **107**, 277202 (2011).
[14] S. F. Caballero-Benitez and I. B. Mekhov, Phys. Rev. Lett. **115**, 243604 (2015).
[15] G. Mazzucchi, W. Kozlowski, S. F. Caballero-Benitez, T. J. Elliott, and I. B. Mekhov, Phys. Rev. A **93**, 023632 (2016).
[16] V. Torggler, S. Krämer, and H. Ritsch, arXiv:1609.06250.
[17] A. J. Kollár, A. T. Papageorge, V. D. Vaidya, Y. Guo, J. Keeling, and B. L. Lev, arXiv:1606.04127.
[18] P. Domokos and H. Ritsch, Phys. Rev. Lett. **89**, 253003 (2002).
[19] D. Nagy, G. Szirmai, and P. Domokos, Eur. Phys. J. D **48**, 127 (2008).
[20] F. Piazza, P. Strack, and W. Zwerger, Ann. Phys. (Amsterdam) **339**, 135 (2013).
[21] A. U. J. Lode and C. Bruder, Phys. Rev. Lett. **118**, 013603 (2017).
[22] J. Keeling, M. J. Bhaseen, and B. D. Simons, Phys. Rev. Lett. **112**, 143002 (2014).
[23] Y. Chen, Z. Yu, and H. Zhai, Phys. Rev. Lett. **112**, 143004 (2014).
[24] F. Piazza and P. Strack, Phys. Rev. Lett. **112**, 143003 (2014).
[25] F. Piazza and P. Strack, Phys. Rev. A **90**, 043823 (2014).
[26] R. M. Sandner, W. Niedenzu, F. Piazza, and H. Ritsch, Europhys. Lett. **111**, 53001 (2015).
[27] H. Habibian, A. Winter, S. Paganelli, H. Rieger, and G. Morigi, Phys. Rev. Lett. **110**, 075304 (2013).
[28] Y. Li, L. He, and W. Hofstetter, Phys. Rev. A **87**, 051604 (2013).
[29] M. R. Bakhtiari, A. Hemmerich, H. Ritsch, and M. Thorwart, Phys. Rev. Lett. **114**, 123601 (2015).
[30] Y. Chen, Z. Yu, and H. Zhai, Phys. Rev. A **93**, 041601 (2016).
[31] N. Dogra, F. Brennecke, S. D. Huber, and T. Donner, Phys. Rev. A **94**, 023632 (2016).
[32] A. E. Niederle, G. Morigi, and H. Rieger, Phys. Rev. A **94**, 033607 (2016).
[33] J. Gelhausen, M. Buchhold, A. Rosch, and P. Strack, SciPost Phys. **1**, 004 (2016).
[34] J. Klinder, H. Keßler, M. R. Bakhtiari, M. Thorwart, and A. Hemmerich, Phys. Rev. Lett. **115**, 230403 (2015).
[35] R. Landig, L. Hruby, N. Dogra, M. Landini, R. Mottl, T. Donner, and T. Esslinger, Nature (London) **532**, 476 (2016).
[36] J. Léonard, A. Morales, P. Zupancic, T. Esslinger, and T. Donner, arXiv:1609.09053.
[37] F. Mivehvar and D. L. Feder, Phys. Rev. A **89**, 013803 (2014).
[38] Y. Deng, J. Cheng, H. Jing, and S. Yi, Phys. Rev. Lett. **112**, 143007 (2014).
[39] B. Padhi and S. Ghosh, Phys. Rev. A **90**, 023627 (2014).
[40] L. Dong, L. Zhou, B. Wu, B. Ramachandhran, and H. Pu, Phys. Rev. A **89**, 011602 (2014).
[41] J.-S. Pan, X.-J. Liu, W. Zhang, W. Yi, and G.-C. Guo, Phys. Rev. Lett. **115**, 045303 (2015).

[42] C. Kollath, A. Sheikhan, S. Wolff, and F. Brennecke, Phys. Rev. Lett. **116**, 060401 (2016).
[43] A. Sheikhan, F. Brennecke, and C. Kollath, Phys. Rev. A **93**, 043609 (2016).
[44] B. Gulácsi and B. Dóra, Phys. Rev. Lett. **115**, 160402 (2015).
[45] W. Zheng and N. R. Cooper, Phys. Rev. Lett. **117**, 175302 (2016).
[46] K. E. Ballantine, B. L. Lev, and J. Keeling, Phys. Rev. Lett. **118**, 045302 (2017).
[47] F. Piazza and H. Ritsch, Phys. Rev. Lett. **115**, 163601 (2015).
[48] J. Zak, Phys. Rev. Lett. **62**, 2747 (1989).
[49] W. P. Su, J. R. Schrieffer, and A. J. Heeger, Phys. Rev. Lett. **42**, 1698 (1979).
[50] T. Holstein, Ann. Phys. (N.Y.) **8**, 325 (1959).
[51] M. Z. Hasan and C. L. Kane, Rev. Mod. Phys. **82**, 3045 (2010).
[52] S. Ryu, A. P. Schnyder, A. Furusaki, and A. W. Ludwig, New J. Phys. **12**, 065010 (2010).
[53] R. Peierls, *Quantum Theory of Solids*, International Series of Monographs on Physics (Clarendon Press, Oxford, 1955).
[54] M. Atala, M. Aidelsburger, J. T. Barreiro, D. Abanin, T. Kitagawa, E. Demler, and I. Bloch, Nat. Phys. **9**, 795 (2013).
[55] K. Baumann, R. Mottl, F. Brennecke, and T. Esslinger, Phys. Rev. Lett. **107**, 140402 (2011).
[56] F. Brennecke, R. Mottl, K. Baumann, R. Landig, T. Donner, and T. Esslinger, Proc. Natl. Acad. Sci. U.S.A. **110**, 11763 (2013).
[57] J. Klinder, H. Keßler, M. Wolke, L. Mathey, and A. Hemmerich, Proc. Natl. Acad. Sci. U.S.A. **112**, 3290 (2015).
[58] R. Resta, Rev. Mod. Phys. **66**, 899 (1994).
[59] R. D. King-Smith and D. Vanderbilt, Phys. Rev. B **47**, 1651 (1993).
[60] S. Ryu and Y. Hatsugai, Phys. Rev. Lett. **89**, 077002 (2002).
[61] See Supplemental Material at http://link.aps.org/supplemental/10.1103/PhysRevLett.118.073602 for derivation of the mean-field equations and the atomic polarization function.